Evidence for Rigid Binding of Rhodamine 6G to Silica Surfaces in Aqueous Solution Based on Fluorescence Anisotropy Decay Analysis

Dina Tleugabulova, Jie Sui, Paul W. Ayers, and John D. Brennan*

Department of Chemistry, McMaster University, Hamilton, ON, L8S 4M1, Canada

Received: September 29, 2004; In Final Form: January 25, 2005

Strong ionic binding of the cationic probe rhodamine 6G (R6G) to the anionic surface of silica particles in water provides a convenient labeling procedure to study both particle growth kinetics and surface modification by time-resolved fluorescence anisotropy (TRFA). The decays for R6G dispersed in diluted Ludox silica sols usually fit to a sum of picosecond and nanosecond decay components, along with a significant residual anisotropy component. The origin of the nanosecond decay component (ϕ_2) is not fully understood, and has been ascribed to wobbling of the probe on the silica surface, the presence of a subpopulation of small nanoparticles in the Ludox sol, or rapid exchange between free and bound R6G. To elucidate the physical meaning of ϕ_2, measurements were performed in various silica-based colloidal systems using different concentrations of silica. We found that the fraction of ϕ_2 was generally higher in Ludox than in aqueous sodium silicate and decreased with increasing silica concentration; ϕ_2 vanished upon gelation of sodium silicate at pH 7 leading to a total loss of R6G depolarization ($r(t) =$ const). These results rule out the presence of local R6G wobbling when bound ionically to colloidal silica and support the rigid sphere model to describe the TRFA decays for R6G−Ludox. This conclusion is entirely supported by steady-state anisotropy data and structural considerations for the R6G molecule and the silica surface.

Introduction

The use of time-resolved fluorescence anisotropy (TRFA) techniques for measuring the dynamic properties of macromolecules relies upon the assumption that the rotation of the fluorescent probe is a good indicator of the overall rotational diffusion of the probe−macromolecule complex. This is true only in cases when the local probe motion, which is independent of the rotation of the macromolecule, has a minimal contribution to the anisotropy decay.[1−5] The presence of local probe motion and the internal flexibility of macromolecules are the most significant problems,[6−13] which make it difficult and often misleading to assign physical significance to the TRFA decay parameters. Vast experimental work is currently in progress to design fluorescent probes that bind rigidly to biomolecules.[14−17] Despite these efforts, the problem of local probe motion is not completely solved,[18] suggesting that it may be an intrinsic property of the covalent bond.[16]

There has recently been significant interest in using TRFA to probe the growth[19−24] and surface modification[25,26] of colloidal silica particles. The rigidity of silica particles removes the problem of internal flexibility found in previous experimental work with macromolecules[6−9] while the ionic labeling of silica with cationic probes seems to overcome the problem of local probe motion.[23,24] Although this latter aspect has not been rigorously tested, the experimental TRFA decays of ionically labeled silica particles are well described by the rigid spherical rotor model developed by Debye[27] and Perrin,[28] and the rotational correlation time measured by TRFA using long-lifetime fluorescent probes is in excellent agreement with the mean particle radius of silica particles present in the silica sol.[23]

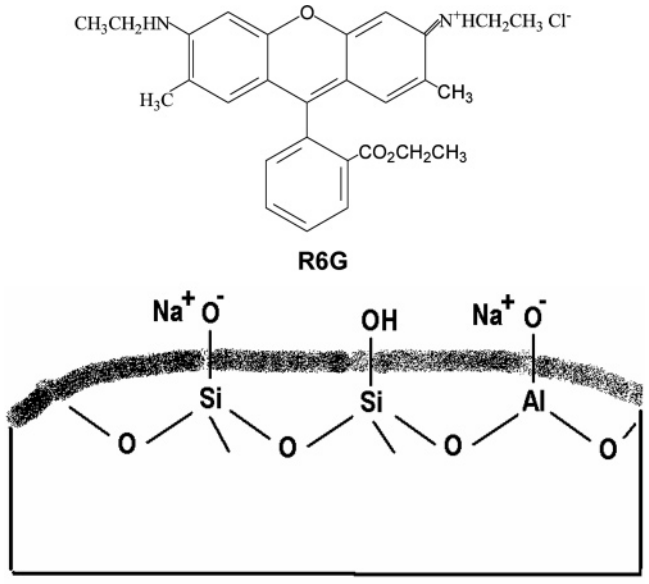

Figure 1. Structures of R6G and Ludox. The thick line denotes the particle surface.

This suggests that the TRFA decay reports on the average diffusional information when applied to a mixture of particles with a normal size distribution.

The most common probe for examination of silica systems by TRFA is rhodamine 6G (R6G, Figure 1), since it has well understood single-lifetime photophysics and a high experimental limiting anisotropy ($r_0 = 0.38$).[29] Since its emission properties do not change upon ionic binding to silica particles,[23−25,30] R6G can be used for monitoring the free and the silica-bound fractions of probe from the same TRFA decay. An issue with the use of

* To whom correspondence should be addressed. Tel: (905) 525-9140 (ext. 27033), Fax: (905) 527-9950, e-mail: brennanj@mcmaster.ca, Internet: http://www.chemistry.mcmaster.ca/faculty/brennan.

10.1021/jp045569r CCC: $30.25
Published on Web 03/31/2005

short-lifetime probes, such as R6G, for silica labeling is that it restricts the TRFA measurement to the rotational diffusion of particles less than 2.5 nm radius.[24] The binding of R6G to larger particles, such as Ludox, leads to significant residual anisotropy ($r_\infty > 0$) in the TRFA decay. The degree of rotation of such particles on the time scale of the R6G intensity decay is insignificant and addressed as a "nondecaying" component.[25,26] This removes the ability to measure the mean particle radius, since much of the particle motion is hidden due to r_∞. However, the fractional contribution from the nondecaying component can be calculated as $g = r_\infty/r_0$,[23] where r_0 is the limiting anisotropy, and can be used to estimate the degree of silica surface modification.[25,26] Besides the g value, two correlation times in a range 0.2−6 ns can be measured with the excited R6G probe.[25,26] The faster correlation time, ϕ_1, of ~ 0.2 ns corresponds to the rotation of free R6G molecules in solution and is therefore attributed to the fraction of free, nonadsorbed R6G molecules in silica sols. The interpretation of the second, slower component (ϕ_2) is less straightforward and has been subjected to different explanations, such as the presence of a subpopulation of small nanoparticles in silica sols and gels,[24,26] the wobbling motion of R6G on the silica surface,[25,26,31] association−dissociation reactions that occur on the time scale of the fluorescence emission of the dye,[29] or a fitting artifact caused by the presence of a particle size distribution in the case of Ludox sols.[23] Whether this component arises solely from the overall rotation of the R6G−Ludox particles or experiences some contribution from the local motion of the R6G dipole relative to the silica surface will influence the choice of a physical model for interpretation of the TRFA parameters. With the correct physical model in place, the practical applications of TRFA can be extended from particle growth kinetics measurements[19−24] and the calculation of the degree of silica surface modification[25,26] to studies of more complex phenomena, such as silica−protein interactions.

In the present paper, we examine the nature of binding of R6G to silica surfaces using experimental TRFA data from several silica systems, including Ludox, sodium silicate (SS), and diglycerylsilane (DGS), and provide supporting data from steady-state anisotropy, transmission electron microscopy, and the theoretical modeling of the R6G−silica interaction to develop a physical model for the origin of the ϕ_2 component, which provides new insight into the interpretation of TRFA data for R6G−silica systems.

Theory

R6G−Ludox as a Mixture of Rotating Spheres. The fundamentals of TRFA analysis are described in detail in the book of Lakowicz.[2] Herein, we provide only specific details of rotational models that apply to the silica systems under study.

In the absence of independent motion of R6G, the time decay of anisotropy $r(t)$ for the probe dipole attached to the surface of silica particles can be modeled as isotropic rotation of k silica spheres of different sizes

$$r(t) = \sum_{i=1}^{i=k} b_i \exp(-t/\phi_i) + r_\infty = r_0^{\exp} \sum_{i=1}^{i=k} f_i \exp(-t/\phi_i) + g r_0^{\exp} \quad (1)$$

where b_i ($0 \le b_i \le r_0$) and ϕ_i are the preexponential constant and rotational correlation time, respectively, corresponding to the rotation of the ith particle,

$$f_i = \frac{b_i \phi_i}{\sum_{i=1} b_i \phi_i} \left(\sum_i f_i = 1,\ 0 \le f_i \le 1\right)$$

is the fractional contribution from ϕ_i to $r(t)$, $r_0^{\exp} = \sum_{i=1}^{i=k} b_i$ is the experimental initial anisotropy at $t = 0$, and $g = r_\infty/r_0^{\exp}$,[23] is the fractional contribution from the nondecaying component. The $r_0^{\exp}$ value indicates the anisotropy after internal conversion and vibrational relaxation, prior to probe rotation, and should nearly correspond to the steady-state anisotropy of R6G in a glassy frozen solvent ($r_0^{\exp} = r_0^{R6G} = 0.38$).[30] The reasons for $r_0^{\exp} < 0.38$ have previously been discussed.[24]

If the particles are normally distributed around a mean radius R, the experimental decay $r(t)$ is biexponential[23]

$$r(t) = f_1 r_0^{\exp} \exp(-t/\phi_1) + f_g r_0^{\exp} \exp(-t/\phi_g) \quad (2)$$

where ϕ_1 is the rotational correlation time of free R6G molecule and ϕ_g ($\phi_g > \phi_1$) reflects the global ("g") tumbling of labeled silica spheres and is related to R by the equation

$$\phi_g = \frac{4\pi R^3 \eta}{3kT} \quad (3)$$

where k is the Boltzmann constant, T is the temperature, and η the viscosity of the solution.

In Ludox AM-30, the particles are size-distributed around a mean particle radius $R = 6$ nm.[32] The labeling of Ludox with the long-lived probe CG437 followed by TRFA measurement and fitting of $r(t)$ to eq 2 gives $\phi_g = 375$ ns, which corresponds to a mean radius of hydrated particles of 7 nm, as calculated from the eq 3.[23] The global tumbling of Ludox spheres cannot be measured by using R6G for labeling because of restrictions imposed on measurable ϕ values by the duration of the excited state ($0.1\tau < \phi < 10\tau$, where τ is the fluorescence lifetime of the probe). As a result, labeling with R6G is feasible for measuring mean particle sizes less than 2.5 nm.[24] In Ludox, the binding of R6G to large particles ($R > 2.5$ nm) leads to significant residual anisotropy, $r_\infty > 0$, and $r(t)$ is described as

$$r(t) = b_1 \exp(-t/\phi_1) + b_2 \exp(-t/\phi_2) + r_\infty = f_1 r_0^{\exp} \exp(-t/\phi_1) + f_2 r_0^{\exp} \exp(-t/\phi_2) + g r_0^{\exp} \quad (4)$$

where $f_1 + f_2 + g = 1$. The global tumbling of Ludox is hidden by r_∞ ("nondecaying" component) and contributes to $r(t)$ with $g = r_\infty/r_0$.[23] In this equation, ϕ_1, b_1, and f_1 account for the possible presence of free R6G molecules in solution, whereas ϕ_2, b_2 and f_2 remain to be attributed to a meaningful rotational mode of R6G in Ludox. Noteworthy in this situation is the fact that the upper part of the normal distribution of particles is "hidden" in the nondecaying component and thus ϕ_2 reflects only the lower part of the distribution and does not provide the average rotational motion of the overall distribution, but only the average of the rotational motions of the lower part of the distribution.

For a rigid sphere,[27,28] the originally polarized emission decays monoexponentially and the time-averaged value of $r(t)$, denoted as the steady-state anisotropy r, is given by the Perrin equation[28]

$$\frac{1}{r} = \frac{1}{r_0}\left(1 + \frac{3\tau}{\phi}\right) \quad (5)$$

where τ is the emission lifetime.

For a mixture of isotropic spheres of different sizes labeled with the same probe with emission lifetime, τ, Weber[33] introduced a relationship between the reduced measure of fluorescence polarization and the spectrum of relaxation processes with rotational correlation times ϕ_i

$$\frac{1/P + 1/3}{1/P_0 + 1/3} = \frac{r_0}{r} = \frac{1}{\sum_i [f_i/(1 + 3\tau/\phi_i)]} \quad (6)$$

where P is the degree of fluorescence polarization and P_0 is the degree of fluorescence polarization for a completely immobile fluorophore determined by its electronic structure. Assuming that only ϕ_1, ϕ_2, and g (eq 4) can be accurately extracted from the anisotropy decay of R6G−Ludox, eq 6 can be rewritten as:

$$\frac{r}{r_0^{\exp}} = \frac{1}{f_1/(1 + 3\tau/\phi_1) + f_2/(1 + 3\tau/\phi_2) + g/(1 + 3\tau/\phi_3)} \quad (7)$$

Rearranging and noting that $3\tau/\phi_3 \approx 0$

$$r = r_0^{\exp}(f/(1 + 3\tau/\phi_1) + (1 - f - g)/(1 + 3\tau/\phi_2) + g) \quad (8)$$

This equation is valid only if ϕ_1, ϕ_2, and g correspond to independent and isotropic rotations of the rigid spheres.

Local Probe Motion. The physical model of a mixture of isotropic spheres, presented above, assumes the absence of local probe motion, which is independent of the global rotation of the Ludox particle. According to this model, ϕ_2 would be attributed to isotropic motion of small silica spheres, which rotate with correlation times on the scale of the intensity decay of R6G. However, if R6G undergoes free rotational diffusion within a cone of semiangle θ, ϕ_2 would be attributed to this wobbling motion. According to the wobble-in-cone model,[34] the order parameter S, which in our case is equal to the g value from eq 4, is related to θ_0

$$S = g = \frac{1}{2}\cos\theta_0(1 + \cos\theta_0) \quad (9)$$

According to eq 9, $g < 1$ in the presence of local probe motion, and thus the condition $g = 1$ ($\theta_0 = 0°$) would rule out the local wobbling of the probe. In R6G−silica systems, the fraction f_1 corresponding to the fast component ϕ_1 is too small ($f_1 \leq 0.01$) to reduce the order parameter significantly ($1 - g = f_1 + f_2$), and thus $g < 1$ is mostly due to the presence of f_2.[25,26,31] Thus, in cases where $f_1 = f_2 = 0$, $g = 1$ and there can be no local probe motion.

Experimental Section

Chemicals. Rhodamine 6G (R6G), poly(acrylic acid) (sodium salt) of $M_w \sim 78\,400$, and poly-L-glutamic acid of $M_w \sim 17\,000$ were purchased from Sigma (St. Louis, MO). Ludox AM-30 (average particle radius of 6 nm, specific surface area of 220 $m^2 \cdot g^{-1}$)[32] was obtained from DuPont. Sodium silicate solution (27 wt % SiO_2, 14 wt % NaOH) and Dowex 50WX8−100 ion-exchange resin of analytical grade were purchased from Aldrich (Milwaukee, WI). Diglycerylsilane (DGS) was prepared from tetramethylorthosilicate (TMOS) as described elsewhere.[35] All water was distilled and deionized using a Milli-Q Synthesis A10 water purification system. All other reagents were used without further purification.

Procedures. All samples were made immediately before analysis. Ludox samples containing 0.75−3 wt % SiO_2 were prepared by diluting Ludox (AM-30; 30 wt % SiO_2; nominal particle radius ≥ 6 nm[32]) in water. DGS sols containing 0.25 wt % SiO_2 were prepared by dissolving 0.21 g of finely ground DGS powder in 20 mL of borate buffer (20 mM, pH 9.2) that was previously cooled to 4 °C. After ~1 min of strong vortexing or sonication, the DGS suspension was filtered through a 0.45 μm membrane filter and the filtrate was doped with R6G to a final concentration of 1 μM. The sample was immediately used for steady state and time-resolved anisotropy measurements, which were repeated at different time intervals. Sodium silicate stock solution (6.4 wt % SiO_2) was prepared by acidification of sodium silicate via reaction with Dowex resin.[36] Sodium silicate samples containing 0.75−3.0 wt % SiO_2 were prepared by diluting the sodium silicate stock solution in 5 mM Tris-HCl, pH 9.2. After mixing, the pH of sodium silicate sols was 7.2. All samples were filtered through a 0.45 μm Acrodisc filter and R6G (1 μM) was added.

Steady-state fluorescence anisotropy measurements were performed at 25 °C using a SLM 8100 spectrofluorimeter (Spectronic Instruments, Rochester, NY) as described elsewhere[37] using $\lambda_{ex} = 495$ nm, $\lambda_{em} = 551$ nm.

Time-resolved fluorescence intensity and anisotropy decays were collected in the time domain mode using an IBH 5000U time-correlated single photon counting fluorimeter (Edinburgh, UK). The measurements were done using a 495-nm NanoLED source run at 1 MHz and an IBH model TBX-04 photon counting PMT detector. The vertically (I_{VV}) and horizontally (I_{VH}) polarized emission components were collected by exciting samples with vertically polarized light while orienting the emission polarizer (Polaroid HNPNB dichroic film) in either a vertical or horizontal direction. Excitation and emission bands were selected with a 500-nm short-pass interference filter (Andover Corporation, AM-49672) and a 515-nm long-pass filter (Andover Corporation, AM-46370). Typically, 1×10^4 counts were collected into the peak channel when the emission polarizer was vertically oriented. The decay histograms were collected over 4096 channels at 22 ps per channel. The horizontal emission decay profile $I_{VH}(t)$ was generated over the same time interval that was used to generate the vertical emission decay profile $I_{VV}(t)$. Samples were held at 25 °C during the measurements. To minimize convolution artifacts, the instrument response profiles were recorded by removing the emission filter and monitoring light scatter from a suspension of Ludox particles in the absence of R6G. The data analysis software corrected the wavelength-dependent temporal dispersion of the photoelectrons by the photomultiplier. The polarization bias (G) of the detection instrumentation was determined by measuring the intensity profiles while the samples were excited with horizontally polarized light and the emission was monitored with a polarizer oriented in the vertical and horizontal directions ($G = 0.65$).

The anisotropy decays were analyzed using the IBH DAS analysis software package, which involves the formation of two related experimental decay curves, $S(t)$ (the "sum" function) and $D(t)$ (the "difference" function)

$$S(t) = I_{VV}(t) + 2GI_{VH}(t) \quad (10)$$

$$D(t) = I_{VV}(t) - GI_{VH}(t) \quad (11)$$

and the experimental anisotropy function is defined as

$$r(t) = \frac{D(t)}{S(t)} = \frac{I_{VV}(t) - GI_{VH}(t)}{I_{VV}(t) + 2GI_{VH}(t)} \quad (12)$$

The *r(t)* decay curve (eq 12) is then analyzed by the reconvolution fitting program for the biexponential hindered rotor model (eq 4) using nonlinear least-squares regression.[38] Attempts were also made to fit the anisotropy decay data to other models, including distributed rotational correlation time models, using Globals WE. However, it was not possible to obtain adequate fits using any of the distribution models provided by Global WE, likely because the use of R6G resulted in sampling of a nonsymmetric distribution of motions, since slower motions associated with large particles are not detected by this probe. Therefore, in all cases the TRFA data was fit to the two-component hindered rotor model provided in the IBH software.

Results and Discussion

TRFA of R6G in Aqueous Silica Sols. In the present work, we studied three aqueous colloidal silica systems: the diglycerylsilane (DGS) sol (0.25 wt % SiO_2) composed of stable primary silica nanoparticles ($R = 1.7$ nm),[24] the sodium silicate (SS) sol, which undergoes continuous polymerization in water[39] and the Ludox sol composed of stable secondary silica particles ($R = 6-7$ nm).[32] For each of these systems, labeled ionically with R6G, the experimental *r(t)* data are fitted to eq 4, in which ϕ_1 and f_1 are attributed to the correlation time and the fraction, respectively, of free R6G molecules present in the silica sol, ϕ_2 and f_2 correspond to the mean correlation time and the fraction, respectively, of silica particles, which rotate on the time scale of the R6G intensity decay, and g corresponds to the fraction of larger particles, whose correlation times are significantly larger than the R6G lifetime. We show how the fitting to eq 4 leads to different equations, which reflect the in situ colloidal state of the system under study.

The TRFA decay of R6G−DGS is shown in Figure 2, and the fits to the decay are provided in Table 1. For R6G−DGS, the fit of *r(t)* to eq 4 leads to $g \approx 0$ (Table 1). This suggests the absence of large secondary particles and interparticle aggregates in the DGS sol, as is indeed the case, as shown by AFM analysis.[24] Hence, based on the fitted results, eq 4 can be rewritten as

$$r(t) = f_1 r_0^{\exp} \exp(-t/\phi_1) + (1 - f_1) r_0^{\exp} \exp(-t/\phi_2) \quad (13)$$

As shown in Table 1, the main contribution to *r(t)* comes from the ϕ_2 component. The value of 4.78 ± 0.02 ns measured 30 min after DGS dissolution corresponds to a mean particle radius of 1.73 ± 0.05 nm,[24] according to eq 3. At longer time intervals, the increase in ϕ_2 is due to further particle growth until a radius of 2.27 ± 0.05 nm is reached after 96 h of aging.

At a higher DGS concentration (0.35 wt % SiO_2), the fit of the experimental *r(t)* data to eq 4 gives $g \approx 0$ and $f_1 < 0.01$ (Figure 2). Hence, most R6G molecules are bound to the silica particles and the decay of $r(t)$ is essentially monoexponential:

$$r(t) = r_0^{\exp} \exp(-t/\phi) \quad (14)$$

Figure 3 shows the TRFA decay for the R6G−SS system. For R6G−SS (Table 1), the fit to eq 4 leads to a significant r_∞ value and the absence of correlation times on the picosecond scale ($f_1 = 0$). This is in good agreement with the fact that the SS sol is composed of polymerized silica particles[40] and R6G is thus adsorbed to the large silica structures. Since these

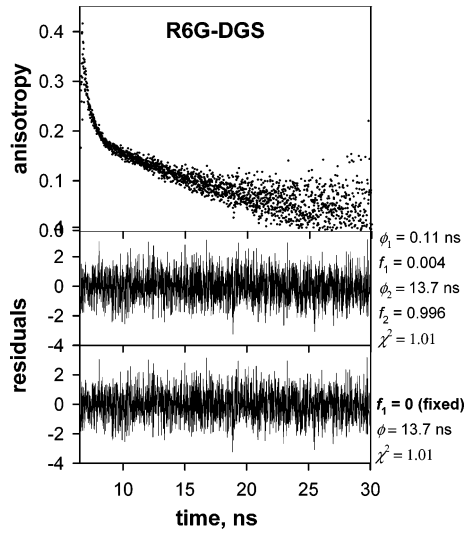

Figure 2. TRFA decay of R6G−DGS in 20 mM borate buffer, pH 9.2. SiO_2, 0.35 wt %; R6G, 1 μM. The upper panel shows the experimental *r(t)* decay curve generated by using eq 12. The middle panel shows the distribution of weighted residuals obtained by the fitting *r(t)* to eq 4. The lower panel shows the distribution of weighted residuals obtained by the forced fitting to eq 14 (f_1 fixed to 0, $g = 0$), indicating that in this system there is essentially no free rotation of R6G.

structures are not expected to reorient on the time scale of the excited state of R6G, the high r_∞ value is well justified. Based on the results of the fit (Table 1), eq 4 can be rewritten as

$$r(t) = (1 - g) r_0 \exp(-t/\phi_2) + g r_0 \quad (15)$$

The absence of ϕ_1 indicates that all R6G molecules are adsorbed to the silica. In this system, ϕ_2 was previously attributed to rotation of single silica nanoparticles entrapped into the pores of the polymerized silica network, whereas the nondecaying component was attributed to the fraction of R6G molecules that were immobilized on the surface of silica walls.[31] As shown in Table 1, the fraction f_2 ($f_2 = 1 - g$) decreases with increasing silica concentration in the sol. This decrease in f_2 occurs under experimental conditions ($SiO_2 > 1.5$ wt %; pH $= 7.2$) that promote fast silica particle growth and polymerization,[31] and for the gelled SS the R6G decay becomes time-independent $r(t) = r_0^{\exp}$ (Table 1). This result indicates that when the amount of free silica particles is decreased due to the polymerization process, the condition $g = 1$ (eq 9) is reached. Importantly, this condition rules out the possibility of ϕ_2 being due to local motion, or "wobbling" of the probe on the silica surface.

Figure 4 shows a typical TRFA decay for the R6G−Ludox system, along with residuals obtained upon fitting of the decay to eq 4. For R6G−Ludox (0.3−0.7 wt % SiO_2), the fit to eq 4 reveals the presence of all three components, ϕ_1, ϕ_2, and g. However, the ϕ_1 component is lost with increasing silica concentration (Table 1), and eq 4 takes the form of eq 15. We relate this effect to the increased uptake of free R6G molecules by silica particles with increasing silica concentration. The nondecaying component is the major contributor to the decay, which is in good agreement with the mean particle radius of 7 nm in water.[23]

The main difference between the decay parameters for R6G in Ludox and in gelled SS, at the same silica concentration, is the absence of ϕ_2 in SS samples (Table 1). The surface area is expected to be larger in the SS gel[31] than in the suspension of nonporous Ludox particles. In SS the probe is thus adsorbed to the walls of the silica network, whereas in Ludox it is bound to

TABLE 1: TRFA Decay Parameters for R6G−DGS (0.25 wt % SiO_2), R6G−Ludox, and R6G−SS[a]

sample	condition	τ, ns	ϕ_1, ns	ϕ_2, ns	r_0^{exp}	r_∞	χ_R^2	g	f_1	f_2
R6G−DGS	30 min[b]	3.95 ± 0.01	0.17 ± 0.02	4.78 ± 0.02	0.366	0.001	1.01	0.003	0.156	0.841
	1 h	3.95 ± 0.01	0.13 ± 0.03	5.32 ± 0.02	0.361	0.001	0.99	0.003	0.021	0.977
	6 h	3.95 ± 0.01	0.16 ± 0.02	6.40 ± 0.02	0.358	0.001	1.00	0.003	0.012	0.985
	48 h	3.95 ± 0.01	0.17 ± 0.01	9.50 ± 0.02	0.367	0.003	0.98	0.009	0.010	0.981
	72 h	3.95 ± 0.01	0.29 ± 0.07	11.50 ± 0.02	0.375	0.001	0.98	0.003	0.009	0.988
	96 h	3.95 ± 0.01	0.17 ± 0.03	11.20 ± 0.02	0.358	0.001	1.03	0.003	0.011	0.986
R6G−SS	0.3 wt % SiO_2 (sol)	3.95 ± 0.01	-	3 ± 1	0.347	0.329	0.99	0.919	0	0.081
	0.7 wt % SiO_2 (sol)	3.94 ± 0.01	-	2.7 ± 0.3	0.360	0.332	0.98	0.923	0	0.077
	1.5 wt % SiO_2 (sol)	3.97 ± 0.01	-	4 ± 1	0.355	0.334	0.98	0.940	0	0.060
	3.0 wt % SiO_2 (gel)	3.96 ± 0.01	-	-	0.350	0.348	1.01	> 0.998	0	< 0.002
R6G−Ludox	0.3 wt % SiO_2	3.92 ± 0.01	0.4 ± 0.1	4 ± 1	0.358	0.286	1.01	0.798	0.019	0.183
	0.7 wt % SiO_2	3.92 ± 0.01	0.3 ± 0.2	3.0 ± 0.4	0.350	0.300	1.01	0.856	0.008	0.136
	1.5 wt % SiO_2	3.93 ± 0.01	-	3.0 ± 0.4	0.360	0.328	0.98	0.915	0	0.085
	3.0 wt % SiO_2	3.92 ± 0.01	-	2.5 ± 0.3	0.361	0.332	0.99	0.921	0	0.079
	6.0 wt % SiO2	3.94± 0.01	-	1.9 ± 0.2	0.350	0.312	0.99	0.891	0	0.011

[a] R6G, 1 μM; solvent, 20 mM borate buffer, pH 9.2 (R6G−DGS), distilled water (R6G−Ludox), and 5 mM Tris-HCl, pH 9.2 (R6G−SS). Excitation, 495 nm; emission, 551 nm. [b] Different time periods after DGS dissolution in 20 mM borate buffer, pH 9.2.

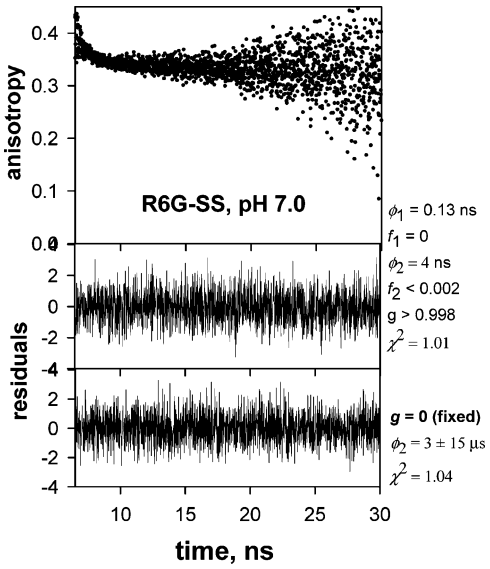

Figure 3. TRFA decay of R6G−SS in 5 mM Tris-HCl, pH 9.2. SiO_2, 3 wt %; R6G, 1 μM. The upper panel shows the experimental *r(t)* decay curve generated by using eq 12. The middle panel shows the distributions of weighted residuals obtained by fitting *r(t)* to the eq 4. The lower panel shows the distribution of weighted residuals obtained by the forced fit of the data to eq 14 ($f_1 = 0$, r_∞ forced to 0). The recovered correlation time of 3 ± 15 μs is statistically insignificant, and is well outside of the range of correlation times measurable using R6G.

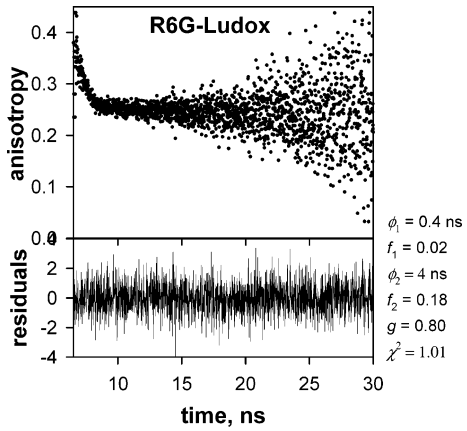

Figure 4. TRFA decay of R6G−Ludox in water. SiO_2, 0.3 wt %; R6G, 1 μM. The upper panel shows the experimental *r(t)* decay curve generated by using eq 12. The lower panel shows the distribution of weighted residuals obtained by fitting *r(t)* to the eq 4. All parameters were allowed to float freely during the fitting.

the surface of discrete particles. If ϕ_2 reflects local probe motion on the silica surface, it should be present in the decay independent of the physical state or concentration of the silica, provided that in the concentration range 0.3−3 wt % SiO_2 the sol microviscosity is not significantly altered.[26] In this case, the presence of ϕ_2 would result in g ≠ 0 (eq 9) and the f_2 value would be constant or higher at increased particle concentrations. Since our results are in disagreement with these expectations, we must attribute ϕ_2 to isotropic rotation of small nanoparticles present in Ludox. According to this conclusion, ϕ_2 and f_2 depend on the fraction of small particles in the silica sol. Particle polymerization would clearly decrease f_2, which is indeed the case for R6G in the gelled SS samples (Table 1).

To better support the interpretation of ϕ_2 being related to small particles, we sought to provide direct evidence for the presence of small silica particles in the Ludox sol. Toward this end, we performed transmission electron microscopy (TEM) on diluted Ludox sols that were cast onto a suitable surface. Dilute sols were utilized to minimize the possibility of aggregation of small particles with radii less than 2 nm during sample preparation. It should also be noted that such particles are near the detection limit of TEM as an imaging method. Nevertheless, we were able to detect particles of ~2 nm radius, as shown in Figure 5a. These small particles were often seen as single particles, attached to the surface of larger particles or forming particle aggregates. As shown in Figure 5b, the Ludox sample was actually composed of a range of particles sizes, covering the region from 1.5 to 9.5 nm radius. The polydispersity of Ludox particles has been previously corroborated by small-angle X-ray scattering techniques,[40−43] and independent studies have reported the presence of small particles (radius, <5 nm).[42,43] Hence, it is likely that the fit to the TRFA decay collapses the normal particle distribution into two categories; particles that are too large to be observed by TRFA (R > 2.5 nm) and those that are sufficiently small to be observable by TRFA (R < 2.5 nm). Since the distribution of observable particles is intrinsically non-Gaussian, it is understandable why the fits of R6G−Ludox to distributed correlation times did not give any statistical improvement over the fits to eq 4 (data not shown).

Ludox-R6G System as a Model of Rigid Spheres. The use of Ludox-R6G as a model for rigid spherical rotors is based on the following assumptions: 1) Ludox particles are uniform, rigid and stable, with no internal surface and no detectable crystallinity; 2) in diluted Ludox sols (≤ 3 wt % SiO_2 in water), silica

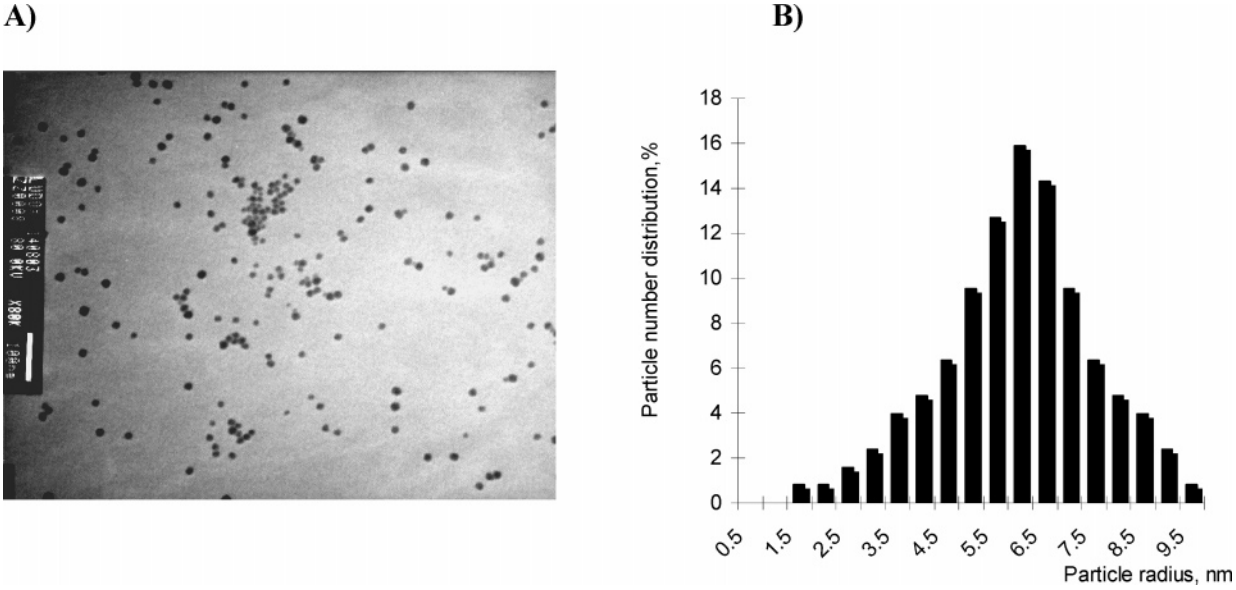

Figure 5. (A) Transmission electron microscopy image of Ludox particles. (B) Particle size distribution of Ludox particles imaged by TEM.

TABLE 2: Fitting Parameters Resulting from Analysis of TRFA Decays for R6G in Aqueous Solutions of DGS (0.25 wt % SiO_2), Ludox (3 wt % SiO_2), Polyacrylic Acid (PAA) and Polyglutamic Acid (PGA)[a]

sample	conditions	ϕ_1, ns	ϕ_2, ns	f_1	f_2	g	r_{calc}	r_{exp}	r_{calc}/r_{exp}
R6G−Ludox	H_2O	0.29	2.88	0.015	0.137	0.848	0.332	0.336	0.99
	0.07 wt % DADMAC	0.18	2.54	0.111	0.300	0.589	0.244	0.240	1.02
	0.15 wt % DADMAC	0.19	2.11	0.395	0.346	0.259	0.120	0.113	1.06
	0.30 wt % DADMAC	0.19	2.01	0.550	0.310	0.140	0.073	0.066	1.11
	2.5 wt % GLTES	0.15	2.31	0.224	0.289	0.487	0.204	0.200	1.02
	2.0 wt % MLTES	0.16	2.10	0.164	0.292	0.544	0.224	0.200	1.12
	0.005 wt % APTES	0.20	2.20	0.725	0.093	0.182	0.079	0.074	1.07
	0.01 wt % APTES	0.17	1.70	0.804	0.110	0.086	0.042	0.040	1.05
R6G−DGS	30 min[b]	0.17	4.61	0.156	0.841	0.003	0.085	0.085	1.00
	1 h	0.13	5.32	0.021	0.977	0.003	0.116	0.115	0.99
	6 h	0.16	6.40	0.012	0.985	0.003	0.135	0.138	1.02
	48 h	0.17	9.50	0.010	0.981	0.009	0.174	0.176	1.01
	72 h	0.29	11.50	0.009	0.988	0.003	0.189	0.185	0.98
	96 h	0.17	11.20	0.011	0.986	0.003	0.189	0.187	0.99
R6G−PAA	0.02 wt %	0.56	3.38	0.193	0.742	0.065	0.090	0.042	2.14
	0.12 wt %	0.83	4.64	0.084	0.848	0.068	0.118	0.090	1.31
R6G−PGA	0.02 wt %	0.19	-	0.974	0	0.026	0.016	0.025	0.64
	0.12 wt %	0.23	-	0.964	0	0.036	0.021	0.026	0.80

[a] R6G Concentration, 1 μM; Excitation, 495 nm; emission, 551 nm. TRFA parameters: r_0^{exp}, 0.35−0.38; ϕ_1, ± 0.01 ns; ϕ_2, ± 0.05 ns; χ_R^2, 0.96−1.05. r_{calc} is calculated using $\tau = 4$ ns and eq 8. r_{exp} (± 0.001) is measured experimentally using continuous excitation at 495 nm. [b] Different time periods after DGS dissolution in 20 mM borate buffer, pH 9.2.

particles rotate independently of each other and the effects of interparticle collisions and repulsions on the rotation are negligible; 3) when dispersed in a diluted Ludox sol, R6G randomly binds to particles of different size; 4) at the probe/particle ratio used, one of every 10 particles is labeled with one R6G molecule; 5) the adsorption of R6G does not modify particle rotation. In the absence of local probe motion, there is a straightforward relationship (eqs 5−8) between the steady-state anisotropy value r and the TRFA parameters. Hence, for R6G−Ludox, we expect a good agreement between experimental r values and those calculated from TRFA data using eq 8. For this comparison, we used TRFA data measured for R6G−Ludox containing different additives, such as diallyldimethylammonium chloride (DADMAC), *N*-(3-triethoxysilylpropyl)-gluconamide (GLTES), *N*-(3-triethoxysilylpropyl)maltonamide (MLTES), and (3-aminopropyl)triethoxysilane (APTES).[26] Depending on their affinity toward the silica surface, these compounds bind to varying degrees, blocking the sites potentially available for R6G adsorption. The competition for the silica surface causes drastic changes in the f_1 and g, but not in ϕ_1 and ϕ_2. These changes in f_1 and g are thus primarily responsible for the decrease in the steady-state anisotropy value due to the modification process (Table 2). As a result, there was a close agreement between experimental r values and those calculated from the TRFA data using eq 8, which supports our assumption that the Ludox-R6G system can be modeled as a collection of rigid spheres. The ϕ_2 component thus reflects the rotation of silica nanoparticles of ∼1.2−1.5 nm radius, which are rigidly labeled with R6G.

There was also the close agreement between experimental r values and those calculated from the TRFA data for R6G−DGS (Table 2), which represents a different colloidal system than Ludox and is described by a different $r(t)$ equation (eq 13). This justifies the use of TRFA for the calculation of the mean particle radius of DGS.[24]

The model of the rigid sphere also requires the rigidity of the labeled host. If R6G is bound to a flexible macromolecule, instead of a Ludox particle, the treatment of such a system as a rigid sphere would be inadequate and thus the Weber equation would not be applicable. To prove this, we added R6G to

aqueous solutions of random-coil anionic polymers, such as poly(acrylic acid) and polyglutamic acid, and measured TRFA decays for the R6G−polymer complexes. The ionic binding of R6G to surfactants and random-coil polyelectrolytes has been reviewed in several recent reports.[44−46] The TRFA decay for R6G−polyglutamic acid was monoexponential (Table 2), showing only the ϕ_1 component. Probably, the binding through a relatively long alkyl side chain does not significantly restrict the mobility of the R6G dipole. The TRFA decay of R6G−poly(acrylic acid) was biexponential with ϕ_2 as a major component. The low g values indicate the absence of rigidity in the polymer chain. As shown in Table 2, there is poor agreement between experimental r values and those calculated from the TRFA parameters, which is consistent with the intrinsically dynamic polymers being improperly described by the model of rigid spheres. Hence, the ability to model silica particles as rigid spheres provides strong evidence that such particles show no internal motion.

Theoretical Analysis of R6G−Silica Interaction from Structural Considerations. The two physical models for the interpretation of TRFA decays assume two different binding modes of the R6G molecule to the silica particle. The wobbling model[34] (eq 9) assumes that the probe dipole is not completely fixed relative to the particle, but rotates with some degree of independence about a bond linking it to the particle. Such partial rotation is to be expected for single-point covalent and ionic conjugates. The model of the rigid sphere is based on the assumption that the R6G dipole maintains a constant orientation relative to the particle axes. This binding mode is expected for probe−particle complexes formed by multiple bonds and several delocalized forces.

From structural considerations, the R6G molecule (Figure 1) has one esterified phenylcarboxyl group and two basic monoethylamino groups, which are formally identical and capable of protonating when they interact with a protic solvent. Hence, in the bulk aqueous phase, the cationic form $(R6G)^+$ is dominant. The phenylcarboxyl and xanthene rings intersect each other with an angle near 90°.[47,48] The main adsorption band of R6G in the visible region corresponds to a transition moment largely parallel to the long axis of the xanthene ring due to a $\pi \rightarrow \pi^*$ transition. Calculation of the atom electron density of R6G using the MOPAC program with a BFGS gradient minimization routine and the MNDO and AM1 Hamiltonians shows that the maximum negative charges in the R6G molecule are on N and O atoms of the ethylamine and COOEt groups, respectively.[49] Hence, R6G interacts with other molecules via either N atoms of the ethylamine group or O atoms of the COOEt group. Assuming that, when using excitation in the visible region, the direction of the transition dipole moment of R6G does not change, it is evident that by using TRFA, we are actually probing the interaction between the xanthene moiety of R6G and the silica surface.

In both resonance structures of R6G (Figure 6), the pK_a of the amine group would resemble that of ammonia (pK_a = 36) while in the other two, one would predict it to be somewhere between that of pyrrole (pK_a = 0.6) and aniline (pK_a = 4.6). In crystal structures of R6G,[50,51] however, both nitrogens have substantial sp^2 character, with the nitrogen lone pair partly delocalized onto the xanthene rings, leaving nitrogen with a partial positive charge. Consequently, the amine/imine hydrogen atoms should be more positively charged than those in most amines, and thus ideally suited for hydrogen bonding.

Possible chemical forms having a potentially higher fluorescence quantum yield than $(R6G)^+$ are a fluorescent dimer[52] and

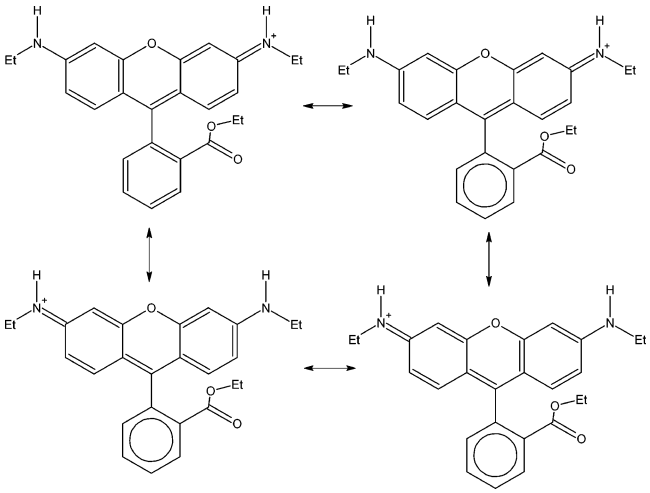

Figure 6. Resonance structures of R6G.

a contact ion-pair of the form $(R6G)^+-A^-$.[53] At the concentration of R6G used in the present study (1 μM), the formation of dimers is negligible in bulk solution.[54] From the absorption spectra (data not shown), we can infer that the relative intensity of the 498−527 nm bands, corresponding to the dimer adsorption, does not change appreciably in the presence of Ludox. This observation rules out any significant increase in aggregation of the dye molecules due to formation of dimers or higher aggregates on the silica surface.

The structures of R6G and Ludox (Figure 1) can be used to rationalize the experimentally observed rigidity of the R6G−Ludox complex. If the positive charge on the imine group is stabilized by the negatively charged silica surface, the symmetry is broken and as a result, the structure in Figure 1 becomes a more accurate representation than its resonance hybrids shown in Figure 6. To support this hypothesis, it is worth noting that the symmetry of the crystal structure of R6G is broken due to hydrogen bonding with the cocrystallized water molecules.[50,51] Examination of the structure of R6G reveals four groups that are available for hydrogen bonding: the two amine/imine groups, the central oxygen, and the ester. If the R6G molecule adsorbs with the xanthene moiety perpendicular to the Ludox surface, the amine/imine hydrogens and the central oxygen atom can all participate in the hydrogen bonding network of the Ludox particle and/or its solvation shell. Unlike ionic bonds, hydrogen bonds are highly directional, and so these interactions will tend to constrain R6G to a rigid geometry relative to the Ludox surface. Nonetheless, the R6G molecule might still "rock" or "wobble" back and forth, rotating about the axis that contains the two amine/imine groups and the central oxygen atom, although the amplitude of the motion will be constrained by the directionality of the interactions tethering these atoms to the surface. For this reason, it seems favorable to tip the xanthene ring system at an angle to the surface and bring the ester moiety toward the Ludox particle, so that the ester can join the hydrogen-bonding network solvating the Ludox particle (Figure 7). If just two of the other three groups formed hydrogen bonds to the surface, then this would totally immobilize the R6G molecule, explaining the experimentally observed results.

The crystal structures seem to indicate that one of the ethylamine groups has more imine character than the other.[50,51] It is useful to ensure, then, that the essential details of the discussion of the previous paragraph would not change even in the extreme case where R6G resembles the structure in Figure 1, rather than a resonance hybrid thereof. Clearly the amine, central oxygen, and ester are still capable of forming hydrogen

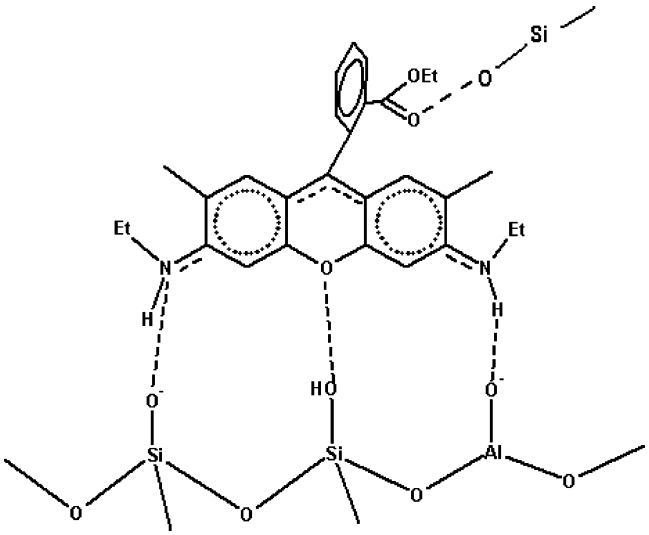

Figure 7. Graphical representation of interactions involved in rigid binding of R6G to the surface of Ludox. Note: The dashed lines indicate hydrogen bonds or ionic bonds to the surface.

bonds to the Ludox surface. The imine can also form hydrogen bonds (through the hydrogen), but the nitrogen atom can also interact directly with water in the solvation shell or, more favorably, the OH or O^- termini of the Ludox surface. Interactions between the imine nitrogen and O^- termini will be especially strong. These interactions may lead to a partial charge transfer from O^- to N^+; if so, one expects the interaction between the imine nitrogen and the surface to be partly ionic and partly covalent.[50,51] Combining this analysis with that of the resonance structures of R6G, it seems that whatever the status of the amine/imine resonance is (and different surface geometries probably favor different structures), there are interactions of sufficient strength, number, and directionality to ensure that motion of R6G is rigidly coupled to that of Ludox particles.

Conclusions

The recent applications of TRFA for the analysis of silica colloids include the nanoparticle metrology approach developed by Geddes[19−23] and the analysis of silica surface modifications developed in our group. Both approaches are based on the assumption that the orientation of the probe dipole relative to the axes of the silica nanoparticle is constant during the measurement. However, this assumption has not been rigorously inspected. The contribution of wobbling motion of R6G on the silica surface or exchange equilibria would be likely reflected by the nanosecond component ϕ_2. Here we show that the fraction of this component is sensitive to the physical state of the sol and the silica concentration. The fact that ϕ_2 vanishes after gelation of SS is the strongest argument against the wobbling of the R6G dipole on the silica surface. In addition, a close agreement between experimental steady-state anisotropy values and those calculated from TRFA parameters, as well as structural considerations, further support the applicability of the model of the rigid spherical rotor to R6G−silica systems. The ϕ_2 component in the decay of R6G−Ludox can thus be attributed to R6G bound to small nanoparticles, and their presence in Ludox was confirmed by TEM analysis.

The present paper also shows that even if the fit of experimental *r(t)* data to eq 4 is done in a model-independent way, the final form of this equation varies depending on the physical state of the colloidal silica. This is the most powerful demonstration of the versatility of TRFA approach to the in situ analysis of nanosize colloids.

Acknowledgment. The authors thank the Natural Sciences and Engineering Research Council of Canada, MDS-Sciex, the Canadian Foundation for Innovation, and the Ontario Innovation Trust for financial support of this work. PA holds the Canada Research Chair in Theoretical Chemistry and Chemical Biology. J.D.B. holds the Canada Research Chair in Bioanalytical Chemistry.

References and Notes

(1) Liu, B. M.; Cheung, H. C.; Mestecky, J. *Biochemistry* **1981**, *20*, 1997.
(2) Lakowitcz, J. R. *Principles of Fluorescence spectroscopy*, 2nd ed.; Kluwer Academic Plenum Publishers: New York, 1999.
(3) Palmer, A. G.; Hochstrasser; R.; Millar, D. P.; Rance, M.; Wright, P. E. *J. Am. Chem. Soc.* **1992**, *115*, 6333.
(4) Kemple, M. D.; Buckley, P.; Yuan, P.; Prendergast, F. G. *Biochemistry* **1997**, *36*, 1678.
(5) Damberg, P.; Jarvet, J.; Allard, P.; Mets, U.; Rigler, R.; Graslund, A. *Biophys. J.* **2002**, *83*, 2812.
(6) Kinosita, K., Jr., Ikegami, A.; Kawato, S. *Biophys. J.* **1982**, *37*, 461.
(7) Vogel, H.; Jaehnig, F. *Proc. Natl. Acad. Sci. U.S.A.* **1984**, *82*, 2029.
(8) Restall, C. J.; Dale, R. E.; Murray, E. K.; Gilbert, C. W.; Chapman, D. *Biochemistry* **1989**, *23*, 6765.
(9) Stein, R. A.; Ludescher, R. D.; Dahlberg, P. S.; Fajer, P. G.; Bennett, R. L. H.; Thomas, D. D. *Biochemistry* **1990**, *29*, 10023.
(10) Van der Heide, U. A., M. A. M. J. Zandvoort, E. van Faassen, G. van Ginkel, and Y. K. Levine. *J. Fluoresc.* **1993**, *3*, 271.
(11) Engelborghs Y. *Spectrochim. Acta A Mol. Biomol. Spectrosc.* **2001**, *57*, 2255.
(12) Phillips D. *Analyst* **1994**, *119*, 543.
(13) Berman, H. A.; Yguerabide, J.; Taylor, P. *Biochemistry* **1985**, *24*, 7140.
(14) Girouard, S.; Houle, M.-H.; Grandbois, A.; Keillor, J. W.; Michnick, S. W. *J. Am. Chem. Soc.* **2005**, *127*, 559.
(15) Adams, S. R.; Campbell, R. E.; Gross, L. A.; Martin, B. R.; Walkup, G. K.; Yao, Y.; Llopis, J.; Tsien, R. Y. *J. Am. Chem. Soc.* **2002**, *124*, 6063.
(16) Dattelbaum, J. D.; Abugo, O. O.; Lakowicz, J. R. *Bioconjugate Chem.* **2000**, *11*, 533.
(17) Corrie, J. E.; Craik, J. S.; Munasinghe, V. R. *Bioconjug Chem.* 1998 Mar-Apr; 9(2): 160.
(18) Mercier, P.; Ferguson, R. E.; Irving, M.; Corrie, J. E.; Trentham, D. R.; Sykes, B. D. *Biochemistry* **2003**, *42*, 4333.
(19) Geddes, C. D.; Birch, D. J. S. *J. Non-Cryst. Solids* **2000**, *270*, 191.
(20) Birch, D. J. S.; Geddes, C. D. *Phys. Rev. E.* **2000**, *62*, 2977.
(21) Geddes, C. D.; Karolin, J.; Birch, D. J. S. *J. Fluoresc.* **2002**, *12*, 113.
(22) Geddes, C. D.; Karolin, J.; Birch, D. J. S. *J. Fluoresc.* **2002**, *12*, 135.
(23) Geddes, C. D. *J. Fluoresc.* **2002**, *12*, 343.
(24) Tleugabulova, D.; Duft, A. M.; Zhang, Z.; Chen, Y.; Brook, M. A.; Brennan, J. D. *Langmuir* **2004**, *20*, 5924.
(25) Tleugabulova, D.; Duft, A. M.; Brook, M. A.; Brennan, J. D. *Langmuir* **2004**, *20*, 101.
(26) Tleugabulova, D.; Zhang, Z.; Chen, Y.; Brook, M. A.; Brennan, J. D. *Langmuir* **2004**, *20*, 848.
(27) Debye, P. *Polar molecules*; Dover: New York, 1929.
(28) Perrin, F. *J. Phys. Radium* **1936**, *7*, 1.
(29) Narang, U.; Wang, R.; Prasad, P. N.; Bright, F. V. *J. Phys. Chem.* **1994**, *98*, 17.
(30) Tleugabulova, D.; Zhang, Z.; Brennan, J. D. *J. Phys. Chem. B* **2003**, *107*, 10127.
(31) Geddes, C. D.; Karolin, J.; Birch, D. J. S. J. *Phys. Chem. B* **2002**, *106*, 3835.
(32) Du Pont. *Ludox Colloidal Silica, Properties, Uses, Storage and Handling*, Data sheet, 1987.
(33) Weber, G. *Biochem. J.* **1952**, *51*, 145.
(34) Kinosita, K., Jr., Ikegami, A.; Kawato, S. *Biophys. J.* **1982**, *37*, 461.
(35) Brook, M. A.; Chen, Y.; Guo, K.; Zhang, Z.; Brennan, J. D. *J. Mater. Chem.* **2004**, *14*, 1469.
(36) Bhatia, R. B.; Brinker, C. J.; Gupta, A. K.; Singh, A. K. *Chem. Mater.* **2000**, *12*, 2434.
(37) Zheng, L.; Reid, W. R.; Brennan, J. D. *Anal. Chem.* **1997**, *69*, 3940.
(38) Imhof, B. *Decay Analysis Software Support Manual*. Version 4. IBH Consultants Ltd, 1989.
(39) Brill, O. L.; Weil, C. G.; Schmidt, P. W. *J. Colloid Interface Sci.* **1968**, *27*, 479.

(40) Brill, O. L.; Weil, C. G.; Schmidt, P. W. *J. Colloid Interface Sci.* **1968**, *27*, 479.
(41) Janosi, A.; Kratky, O.; Sekora, A. *Monatsh. Chem.* **1969**, *100*, 1973.
(42) Walter, G.; Kranold, R.; Baldrian, J.; Steinhart, M. *J. Appl. Crystallogr.* **1985**, *18*, 205.
(43) Axelos, M. A. V.; Tchoubar, D.; Bottero, J. Y. *Langmuir* **1989**, *5*, 1186.
(44) Hamai, S.; Sasaki, K. *Microchem. J.* **2001**, *69*, 27.
(45) DeLaCruz, J. L.; Blanchard, G. L. *J. Phys. Chem. B* **2003**, *107*, 7102.
(46) Deshpande, A. V.; Namdas, E. B. *Appl. Phys. B* **1997**, *64*, 419.
(47) Abrahams, M. J.; Picher, D. H.; Fackler, P. H.; Lock, C. J.; Howard-Lock, H. E.; Faggiani, R.; Teher, B. A.; Richmond, R. C. *Inorg. Chem.* **1986**, *25*, 3980.
(48) Kvick, A.; Vaughan, G. B. M.; Wang, X.; Sun, Y.; Long, Y. *Acta Crystallogr.* **2000**, *C56*, 1232.
(49) Saini, G. S. S.; Kaur, S.; Tripathi, S. K.; Mahajan, C. G.; Thanga, H. H.; Verma, A. L. *Spectrochim. Acta Part A* **2005**, *61*, 653.
(50) Adhikesavalu, D. N.; Mastropaolo, D.; Camerman, A.; Camerman, N. *Acta Crystallogr.* **2001**, *C57*, 657.
(51) Fun, H.-K.; Chinnakali, K.; Sivakumar, K.; Lu, C. M.; Xiong, R. G.; You, X. Z. *Acta Crystallogr.* **1997**, *C53*, 1619.
(52) Kemnitz, K.; Yoshihara, K. *J. Phys. Chem.* **1991**, *95*, 6095.
(53) Ferreira, J. A. B.; Costa, S. M. B. *Chem. Phys. Lett.* **1999**, *307*, 139.
(54) Tapia Estevez, M. J.,; Lopez Arbeloa, F.; Lopez Arbeloa, T.; Lopez Arbeloa, I. *Langmuir* **1993**, *9*, 3629.